



OPEN ACCESS

EDITED BY

Thorsten Jürgen Maier,
Paul-Ehrlich-Institut (PEI), Germany

REVIEWED BY

Md A. Hakim,
National Institutes of Health (NIH),
United States
Geneviève Pépin,
Université du Québec à Trois-Rivières,
Canada
Adriana R. Silva,
Oswaldo Cruz Foundation (Fiocruz), Brazil

*CORRESPONDENCE

Jianning Zhang
✉ jianningzhang@hotmail.com
Xin Chen
✉ xinchentianjin@163.com
Shu Zhang
✉ zhangshu2017@tmu.edu.cn

†These authors have contributed equally to this work

SPECIALTY SECTION

This article was submitted to
Inflammation,
a section of the journal
Frontiers in Immunology

RECEIVED 16 December 2022

ACCEPTED 31 March 2023

PUBLISHED 14 April 2023

CITATION

Cao Y, Shi M, Liu L, Zuo Y, Jia H, Min X, Liu X, Chen Z, Zhou Y, Li S, Yang G, Liu X, Deng Q, Chen F, Chen X, Zhang S and Zhang J (2023) Inhibition of neutrophil extracellular trap formation attenuates NLRP1-dependent neuronal pyroptosis *via* STING/IRE1 α pathway after traumatic brain injury in mice.
Front. Immunol. 14:1125759.
doi: 10.3389/fimmu.2023.1125759

COPYRIGHT

© 2023 Cao, Shi, Liu, Zuo, Jia, Min, Liu, Chen, Zhou, Li, Yang, Liu, Deng, Chen, Chen, Zhang and Zhang. This is an open-access article distributed under the terms of the [Creative Commons Attribution License \(CC BY\)](https://creativecommons.org/licenses/by/4.0/). The use, distribution or reproduction in other forums is permitted, provided the original author(s) and the copyright owner(s) are credited and that the original publication in this journal is cited, in accordance with accepted academic practice. No use, distribution or reproduction is permitted which does not comply with these terms.

Inhibition of neutrophil extracellular trap formation attenuates NLRP1-dependent neuronal pyroptosis *via* STING/IRE1 α pathway after traumatic brain injury in mice

Yiyao Cao^{1,2,3†}, Mingming Shi^{1,2,3†}, Liang Liu^{1,2,3†}, Yan Zuo^{4†}, Haoran Jia^{1,2,3}, Xiaobin Min⁵, Xilei Liu^{1,2,3}, Zhijuan Chen^{1,2,3}, Yuan Zhou^{1,2,3}, Shenghui Li^{1,2,3}, Guili Yang^{1,2,3}, Xiao Liu^{1,2,3}, Qianjun Deng^{1,2,3}, Fanglian Chen^{2,3}, Xin Chen^{1,2,3*}, Shu Zhang^{1,2,3*} and Jianning Zhang^{1,2,3*}

¹Department of Neurosurgery, Tianjin Medical University General Hospital, Tianjin, China, ²Key Laboratory of Post-trauma Neuro-repair and Regeneration in Central Nervous System, Tianjin Neurological Institute, Ministry of Education, Tianjin, China, ³Tianjin Key Laboratory of Injuries, Variations and Regeneration of Nervous System, Tianjin Neurological Institute, Tianjin, China, ⁴Department of Geriatrics, Tianjin Medical University General Hospital, Tianjin, China, ⁵Baodi Clinical College, Tianjin Medical University, Tianjin, China

Introduction: Increased neutrophil extracellular trap (NET) formation has been reported to be associated with cerebrovascular dysfunction and neurological deficits in traumatic brain injury (TBI). However, the biological function and underlying mechanisms of NETs in TBI-induced neuronal cell death are not yet fully understood.

Methods: First, brain tissue and peripheral blood samples of TBI patients were collected, and NETs infiltration in TBI patients was detected by immunofluorescence staining and Western blot. Then, a controlled cortical impact device was used to model brain trauma in mice, and Anti-Ly6G, DNase, and CL-amidine were given to reduce the formation of neutrophilic or NETs in TBI mice to evaluate neuronal death and neurological function. Finally, the pathway changes of neuronal pyroptosis induced by NETs after TBI were investigated by administration of peptidylarginine deiminase 4 (a key enzyme of NET formation) adenovirus and inositol-requiring enzyme-1 alpha (IRE1 α) inhibitors in TBI mice.

Results: We detected that both peripheral circulating biomarkers of NETs and local NETs infiltration in the brain tissue were significantly increased and had positive correlations with worse intracranial pressure (ICP) and neurological dysfunction in TBI patients. Furthermore, the depletion of neutrophils effectively reduced the formation of NET in mice subjected to TBI. We found that degradation of NETs or inhibition of NET formation significantly inhibited nucleotide-binding oligomerization domain (NOD)-like receptor pyrin domain

containing 1 (NLRP1) inflammasome-mediated neuronal pyroptosis after TBI, whereas these inhibitory effects were abolished by cyclic GMP-AMP (cGAMP), an activator of stimulating Interferon genes (STING). Moreover, overexpression of PAD4 in the cortex by adenoviruses could aggravate NLRP1-mediated neuronal pyroptosis and neurological deficits after TBI, whereas these pro-pyroptotic effects were rescued in mice also receiving STING antagonists. Finally, IRE1 α activation was significantly upregulated after TBI, and NET formation or STING activation was found to promote this process. Notably, IRE1 α inhibitor administration significantly abrogated NETs-induced NLRP1 inflammasome-mediated neuronal pyroptosis in TBI mice.

Discussion: Our findings indicated that NETs could contribute to TBI-induced neurological deficits and neuronal death by promoting NLRP1-mediated neuronal pyroptosis. Suppression of the STING/ IRE1 α signaling pathway can ameliorate NETs-induced neuronal pyroptotic death after TBI.

KEYWORDS

neutrophil extracellular trap, traumatic brain injury, pyroptosis, NLRP1, STING, IRE1 α

Introduction

Traumatic brain injury (TBI) is one of the leading causes of death and disability among all age groups worldwide (1). Following the primary brain injury, the secondary brain injury of TBI is associated with poor neurological outcomes, for which there is no effective treatment (2). TBI-induced neuronal death at the site of injury appears to be the consequence of both the primary brain injury and the secondary brain injury, depending on its localization and temporal course. Neuroinflammation orchestrated by cerebral glia was reported to play a critical role in the pathological process after TBI (3). However, emerging evidence suggested that neuronal cell is also involved in immune responses in brain injury, such as nucleotide-binding oligomerization domain (NOD)-like receptor pyrin domain containing 1 (NLRP1) and NLRP3 inflammasome-mediated inflammation (4, 5). However, the molecular mechanisms responsible for inflammasome-induced neuronal cell death and neuronal inflammation following TBI are complex and still poorly understood.

Pyroptosis, as a novel form of programmed cell death, is characterized by inflammasome-promoted and caspase-1 and/or -11-dependent rapid collapse and gasdermin D (GSDMD)-mediated rupture of cellular integrity, osmotic swelling, and release of pro-inflammatory IL(interleukin)-1 β and IL-18 (6). Classically, three types of inflammasomes have currently been validated as playing a major role in the context of neurotrauma (7, 8): NLRP1, NLRP3, and absent in melanoma-2 (AIM2). In the brain, NLRP1 inflammasomes are validated to be primarily expressed in neurons (9). Multiple lines of evidence have confirmed that targeting inhibition of inflammasome priming and activation are critical for ameliorating neuronal cell death and neuroinflammation in secondary brain injury following TBI (10–

12). Therefore, targeting NLRP1 inflammation-mediated neuronal pyroptosis may provide new insight and a theoretical basis for developing an effective therapy for TBI.

Since neutrophil extracellular traps (NETs) were first reported by Brinkman in 2004, the NET formation has been reported to be involved in the pathophysiological processes of various brain injuries, such as TBI (13). NETs an extracellular web-like structure released by neutrophils are composed of extracellular double-stranded DNA combined with several components, including histones, myeloperoxidase (MPO), neutrophil elastase, and cathepsin (14). NETs are generated upon excessive neutrophil activation for trapping a broad range of pathogens, including bacteria and viruses, and helping fight infection (15). However, excessive NET formation is generally considered a double-edged sword of innate immunity (16). Excessive NET formation has been recently identified as a novel mechanism contributing to the exacerbation of inflammation (17), the onset of autoimmune disorders (18), and thrombi formation (19). NETs have been reported to be existed in the brain parenchyma (20) and cerebrovascular thrombi (21) of ischemic stroke patients and inhibition of NET formation could improve stroke outcomes in mice subjected to ischemic stroke (20). In addition, previous studies have found that NETs can contribute to brain edema and neurological deficits (22). However, whether NETs are present in the brain tissue of TBI patients, and the biological function and underlying mechanism of NETs in TBI-induced neuronal cell death are still not fully understood.

DNA released by NETs is one of the main sources of circulating free DNA after TBI, and it plays a biological role by activating a series of DNA sensors in the cytosol. Cyclic guanosine 5'-monophosphate (GMP)-adenosine 5'-monophosphate (AMP) synthase (cGAS) is generally considered a crucial cytoplasmic DNA receptor that senses and is stimulated with the combination

of endogenous and exogenous double-stranded DNA (dsDNA) (23). cGAS then catalyzes a reaction between guanosine triphosphate (GTP) and adenosine triphosphate (ATP) to produce a second messenger cyclic GMP-AMP (cGAMP), which activates the adaptor protein stimulating Interferon genes (STING) (24). STING is a transmembrane protein located on the endoplasmic reticulum (ER) that functions by regulating innate immunity and sensing pathogens primarily by regulating tank-binding kinase 1 (TBK1)/I interferon regulatory factor 3 (IRF3)/type I interferons (IFNs) pathway (24). Recently studies have revealed that STING not only provokes the TBK1/IRF3/IFNs pathway in a classical way but also is involved in the activation of ER stress and unfolded protein response (UPR) (25–27). STING has been reported to play an important role in regulating the neuroinflammatory process and pyroptosis after TBI (28, 29), but its effects on NLRP1 inflammasome-mediated neuronal cell death have not been explored in TBI. Interestingly, Inositol-requiring enzyme-1 alpha (IRE1 α), one of the sensor proteins in the endoplasmic reticulum associated with ER stress, has been shown to regulate NLRP1-mediated neuronal pyroptosis in a neonatal hypoxic-ischemic encephalopathy rat model (30).

In the present study, we hypothesized that NET formation promotes neuronal pyroptosis and neuronal cell death *via* STING/IRE1 α pathway after induction of TBI in mice.

Methods

Human brain tissues

Human brain tissues were obtained in accordance with an ethically reviewed and approved protocol from Tianjin Medical University General Hospital. Four patients with severe TBI, defined as post-resuscitation Glasgow coma scale (GCS) scores less than 8, were included. Control brain specimens were obtained from three patients with glioma who underwent maximizing resection of malignant glioma to improve survival. None of the patients had any other known neurological disorder. The demographics and clinical characteristics of these patients are shown in [Supplemental Table 1](#).

Quantification of NETs

Plasma was collected from the whole blood of humans by centrifugation at $250 \times g$ for 20 min. Plasma DNA was quantified according to the manufacturer's instructions using the Quant-iT PicoGreen dsDNA Assay kit (P11496, Invitrogen). We also developed a capture ELISA based on citrullinated histone H3 associated with DNA (H3cit-DNA complex), as reported previously (31). For the capture of antibodies, 5 μ g/ml anti-H3Cit (ab5103, Abcam, UK) was coated onto 96-well plates overnight at 4 $^{\circ}$ C. The plates were then blocked with 5% BSA for 2 h at room temperature. After being washed with washing buffer (300 μ L each), 50 μ L of plasma was added into the wells with 80 μ L incubation buffer containing a peroxidase-labeled anti-DNA mAb (Cell Death

ELISA, 11774425001, Roche, Basel, Switzerland). The plates were then incubated at room temperature for 2 h. After being washed six times, the plate was developed with 100 μ L ABST substrate. The absorbance (OD) at 450 nm was measured after 30 min incubation in the dark.

Animals

Male C57BL/6 mice (8–10 weeks old and 25–30g), were purchased from the Experimental Animal Laboratories of the Academy of Military Medical Sciences (Beijing, China). All mice were housed in a temperature (20 $^{\circ}$ C–24 $^{\circ}$ C) and humidity (50%–60%) controlled environment with food and water available *ad libitum* under a standard 12-h light/dark cycle. All experimental procedures were conducted in strict accordance with the National Institutes of Health Guide for the Care and Use of Laboratory Animals and approved by Tianjin Medical University Animal Care and Use committee.

Experimental design

All experimental mice were randomly assigned to five experimental groups. Surgeries, histological, and neurological function assessments were carried out in a blinded manner.

Experiment 1

To examine the role of neutrophils in secondary neuronal cell death following TBI, 36 mice were randomly assigned into the following three groups (n=12/group): sham, TBI + Isotype, and TBI + Anti-Ly6G for western blot analysis and histological analysis. To assess the role of neutrophils in neurological function after TBI, a total of 36 mice were randomly divided into three groups (n=12/group): sham, TBI + Isotype, and TBI + Anti-Ly6G. On days 1, 3, 5, and 7 post-injuries, the rotarod test and modified neurological severity score (mNSS) were conducted to assess post-trauma motor functions.

Experiment 2

To investigate the effects of neutrophil extracellular trap and Stimulators of interferon genes (STING) agonist in secondary neuronal cell death following TBI, 48 mice were randomly assigned into the following four groups (n=12/group): sham, TBI + vehicle, TBI + DNase 1, and TBI + DNase 1 + cGAMP for western blot analysis and histological analysis.

Experiment 3

To investigate the effects of neutrophil extracellular trap formation inhibitor and STING agonist in secondary neuronal cell death following TBI, 48 mice were randomly assigned into the following four groups (n=12/group): sham, TBI + vehicle, TBI + Cl-amidine, and TBI + Cl-amidine + cGAMP for western blot analysis and histological analysis. To assess the effects of neutrophil extracellular trap formation inhibitor and STING agonist in

neurological function after TBI, a total of 48 mice were randomly divided into four groups (n=12/group): sham, TBI + Isotype, and TBI + Anti-Ly6G. On days 1, 3, 5, and 7 post-injuries, the rotarod test and mNSS were conducted to assess post-trauma motor functions.

Experiment 4

To determine the effects of neutrophil extracellular trap formation and STING inhibitor in secondary neuronal cell death following TBI, 48 mice were randomly assigned into the following four groups (n=12/group): sham, TBI + Ad-con, TBI + Ad-PAD, and TBI + Ad-PAD + C-176 for western blot analysis and histological analysis.

Experiment 5

To further explore the IRE1 α signaling pathway in neutrophil extracellular traps-mediated neuronal pyroptosis after ICH, a total of 24 mice were randomized into four groups (n=6/group): sham, TBI + Ad-con, TBI + Ad-PAD, and TBI + Ad-PAD + kira6 for western blot analysis. To assess the IRE1 α signaling pathway in neurological function after TBI, 48 mice were randomly divided into four groups (n=12/group): sham, TBI + Ad-con, TBI + Ad-PAD, and TBI + Ad-PAD + kira6. On days 1, 3, 5, and 7 post-injuries, the rotarod test and mNSS were conducted to assess post-trauma motor functions.

TBI model

TBI was induced by a digital electromagnetically controlled cortical impact (CCI) device (CCI-6.3 device, Custom Design & Fabrication, USA) as previously described (32). Briefly, each mouse was anesthetized with 1–1.5% isoflurane in 30% oxygen and 70% nitrous oxide during the surgical procedure, and the body temperature was maintained at $37 \pm 0.5^\circ\text{C}$ using a heating blanket. After fixation on a custom head-fixing apparatus, a craniotomy was performed using a high-speed micro drill on the right parietal cortex (2.5 mm posterior from the bregma and 2.5 mm lateral to the sagittal suture) (33). A 4-mm-flat impactor tip was used to conduct a unilateral 2.2 mm depth impact on the mice at 5 m/s with a 200 ms dwell time. The sham mice were subjected to the same surgical procedure without the infliction of CCI. All procedures were performed with a strict aseptic technique.

Injection of adenoviruses

Recombinant PAD4 adenovirus (Adeno-PAD4; Adeno-CMV-Padi4-3*flag-tagged SV40-EGFP, 4×10^{10} plaque-forming-unit/mL) and empty adenovirus (Adeno-CMV-3*flag-tagged SV40-EGFP) were purchased from Genechem (Shanghai, China). A total of 4 μL of Adeno-PAD4 (Ad-PAD4) or Adeno-EGFP (Ad-con) was injected stereotactically into two sites of the right cortex (1.5 mm caudal and 1.5 mm rostral from lesion epicenter) at a dose of 2 μL , respectively, 24 h before mice subjected to CCI. The

injections were performed with a 5 μL Hamilton syringe (Hamilton Company, USA) at a flow rate of 0.5 $\mu\text{L}/\text{min}$ through the hole at a depth of 1.0 mm (33, 34). After the injection, the needle was held for 10 min before retraction, and the scalp was stitched.

Neutrophil depletion

As previously described (35), to deplete neutrophils *in vivo*, each mouse received an intraperitoneal (i.p.) injection of 100 μg monoclonal anti-mouse Ly6G antibody (1A8 clone; specific for neutrophils, BE0075-1, BioXCell, NH) 24 h before TBI and 24 h after TBI. Each control mouse received 100 μg of the isotype antibody rat IgG2a in the same manner.

Drug administration

Human recombinant DNase 1 treatment

As previously described (13), mice were intravenously (i.v.) injected with 5 mg/kg rh DNase 1 (Deoxyribonuclease 1 human recombinant; enz-319-10,000 IU, ProSpec-Tany TechnoGene Ltd., Rehovot, Israel) or vehicle (8.77 mg/mL sodium chloride and 0.15 mg/mL calcium chloride) 1 h after TBI and then injected daily until the mice were euthanized.

Peptidyl arginine deiminases inhibitor treatment

A stock solution of the PAD inhibitor, Cl-amidine (GC35706, GLPBIO, USA), was diluted in saline (5% v/v). Then, as previously mentioned (13), mice were assigned to the injection intraperitoneally of Cl-amidine at a dose of 10 mg/kg or an equal volume of vehicle (saline containing 5% DMSO) 10 min after TBI and once per day for three consecutive days.

Stimulators of interferon genes antagonist administration

The STING antagonist C-176 (S6575, Selleck, USA) was dissolved in a stock solution containing 5% dimethyl sulfoxide (DMSO) and 95% corn oil and then diluted in saline (5% v/v). As previously reported (29), 10 mg/kg C-176 or an equal volume of vehicle (saline containing 5% stock solution) was administered i.p. 1 h after TBI and once per day for three consecutive days.

2'3'-cGAMP treatment

As previously reported (36, 37), 1 mg/kg 2'3'-cGAMP (tlr-Inacga23-1; *In vivo*Gen, San Diego, USA) or vehicle (phosphate-buffered saline, PBS) was administered intravenously 10 min before TBI and once per day for three consecutive days.

Inositol-requiring enzyme 1 α inhibitor administration

The IRE1 α inhibitor kira6 (S8658, Selleck, USA) was dissolved in a stock solution containing 5% DMSO, 30% Tween-80, and 65% corn oil and then diluted in saline (5% v/v). As previously reported (38), 10 mg/kg kira6 or an equal volume of vehicle (saline

containing 5% stock solution) was administered i.p. 1 h after TBI and once per day for three consecutive days.

Neurological assessment

Neurological function was evaluated at 1, 3, 5, and 7 d after TBI using the well-established mNSS, as described previously (39). The mNSS consists of a motor (muscle state and abnormal action), sensory (visual, tactile), reflex, and balance tests. The higher score represents the more serious neurological impairment (normal score, 0; maximal score, 18).

Rotarod test

As described previously (40), the rotarod test was performed to assess the sensorimotor function, coordination, and balance at 1, 3, 5, and 7 d post-injury with an accelerating Rota-rod apparatus (RWD Life Science, Shenzhen, China). Before induction of CCI, mice in each group were trained for three consecutive days. Each mouse was placed in each lane on the rotating cylinder, which accelerated from 4 to 40 rpm/min within 5 min. The latency to fall for each mouse was recorded. Each mouse was tested three times with an interval of 30 min between trials, and the average latency to falling was used for analysis.

H&E staining

H&E staining was performed to evaluate damaged cells as previously described (41). The paraffin-embedded 4% paraformaldehyde-fixed brains were sliced into 10 μm thick sections. The brain sections were then deparaffinized with xylene and dehydrated in a graded series of alcohols. Sections were incubated with hematoxylin (Sigma Aldrich) for 3 mins and washed three times with PBS. Then, sections were stained with eosin for 4 min. The average number of normal neurons and damaged neurons were calculated by ImageJ software (Version 1.46r, Wayne Raband, USA).

Nissl staining

Nissl staining was performed to evaluate neuronal damage as previously described (32). The paraffin-embedded 4% paraformaldehyde-fixed brains were sliced into 10 μm thick sections. The brain sections were then deparaffinized with xylene and dehydrated in a graded series of alcohols. Sections were incubated with Nissl staining solution (Sigma Aldrich) for 20 mins at 60°C in the oven. The damaged neurons were characterized by a shrunken cytoplasm and condensed staining, while normal neurons were characterized by a large and full soma. The average number of normal neurons and damaged neurons were calculated by ImageJ software (Version 1.46r, Wayne Raband, USA).

Immunofluorescence staining

After the sacrifice of mice, the brains were removed and immersed in 4% paraformaldehyde, 15% sucrose, and 30% sucrose to complete fixation and dehydration. Brains were then sliced into 8 μm-thick coronal sections using a cryostat (Leica, Model CM1950, Germany). After being washed in PBS, the sections were permeabilized with 0.1% Triton X-100 (Sigma Aldrich) for 30 mins and incubated with 3% BSA for 1 h at room temperature. Thereafter, sections were incubated overnight at 4°C with primary antibodies, including mouse anti-NeuN (1:1000, ab104224), rabbit anti-NeuN (1:1000, ab177487), rabbit anti-H3Cit (1:1000, ab5103, all from Abcam, UK), rabbit anti-STING (1:500, 13647, Cell Signaling Technology), goat anti-MPO (1:500, AF3667, R&D Systems), goat anti-CD31 (1:200, AF3628, R&D Systems), rat anti-mouse Ly6G (1:200, 551459, BD Biosciences), mouse anti-Caspase1 (1:500, sc-56036, Santa Cruz Biotechnology), mouse anti-NLRP1 (1:500, sc-390133, Santa Cruz Biotechnology). The sections were then incubated with the species-appropriate Alexa Fluor-conjugated IgG (1:500, Invitrogen, USA) for 1 h at room temperature. DNA was stained with 4',6-diamidino-2-phenylidole (DAPI, Abcam). Staining was visualized and captured by an inverted fluorescence microscope (Olympus, Japan). Images were then analyzed using ImageJ software (Version 1.46r, Wayne Raband, USA).

Terminal deoxynucleotidyl transferase dUTP nick-end labeling assay

For quantification of neuronal apoptosis at 3 days after TBI, double staining of neuron marker NeuN (red) and TUNEL (green) was conducted using the *In Situ* Cell Death Detection kit (Roche, South San Francisco, CA, USA), according to the manufacturer's instructions. Coronal sections were counterstained with mouse anti-NeuN (1:1000, ab104224, Abcam, UK), at 4°C overnight and subsequently incubated with the *In Situ* Cell Death Detection kit and a secondary donkey anti-mouse Alexa 594 antibody for 1 h at 37°C in the dark. The average number of TUNEL-positive neurons in the contused cortex was calculated by ImageJ software (Version 1.46r, Wayne Raband, USA).

Western blot analysis

Total proteins in the brain tissues of TBI mice were extracted using RIPA lysis buffer (Sigma-Aldrich, MO, USA). Proteins were separated by sodium dodecyl sulfate-polyacrylamide gel electrophoresis (SDS-PAGE) and transferred to a 0.45 μm pore size polyvinylidene difluoride (PVDF) membranes (Millipore, Temecula, CA, USA). The membranes were blocked with 5% skimmed milk for 2 h and then incubated primary antibodies: including rabbit anti-IREα (1:1000, 3294), rabbit anti-ASC (1:1000, 67824), rabbit anti-Histone H3 (anti-H3; 1:1000, 9715), rabbit anti-STING (1:1000, 13647), rabbit anti-β-actin (1:2000, 4970, all from

Cell Signaling Technology, MA), rabbit anti-H3Cit (1:1000, ab5103), rabbit anti-p-IRE α (1:1000, ab124945), rabbit anti-IL-18 (1:1000, ab207323), rabbit anti-MPO (1:1000, ab208670), rabbit anti-PAD4 (1:1000, ab96758, all from Abcam, UK), anti-Caspase1 (22915-1-AP, 1:2000, Proteintech Group, Wuhan, China), anti-GSDMD (AF4012, 1:2000, Affinity Biosciences), mouse anti-NLRP1 (1:500, sc-390133, Santa Cruz Biotechnology). The membranes were then washed three times and incubated with species-appropriate horseradish peroxidase (HRP)-conjugated secondary antibodies (1:5000, Cell Signaling Technology, USA) for 1h at room temperature. Finally, the immunoblot bands were visualized using ECL under an imaging system (Bio-Rad, Hercules, CA, USA). Protein quantification was measured in optical density units using Image Lab-5.2.1 software (Bio-Rad, CA, USA) and was normalized to the corresponding sample expression of β -actin.

Statistical analysis

All statistical analysis was performed with Graph-Pad Prism software (Graph Pad Software, Version8.1.2 San Diego, CA, USA). Multiple comparisons were analyzed by one-way analysis of variance (ANOVA) followed by Tukey's multiple comparison *post*

hoc test. The results were expressed as means \pm (SD). Comparison between 2 groups was performed by unpaired Student's t-test or Mann-Whitney test. A value of $P < 0.05$ was considered statistically significant.

Results

NETs formation correlates with elevated ICP and worse neurological function in TBI patients

To explore whether neutrophils are present in the brain tissues of TBI patients, we obtained brain specimens from four severe TBI patients who underwent a decompressive craniotomy to remove the hematoma and/or to reduce life-threatening high intracranial pressure. We found that infiltration of both neutrophils and neutrophils-derived NETs was significantly increased in the brain tissues of TBI patients (Figures 1A, B). A typical head CT image of a patient with TBI observed a brain contusion in the right frontal lobe with intracranial hematoma (Figure 1C). Plasma cell-free DNA (cf-DNA) (Figure 1D), a rough biomarker of NETs, and plasma H3Cit-DNA complex (Figure 1E), a specific biomarker of NETs, were

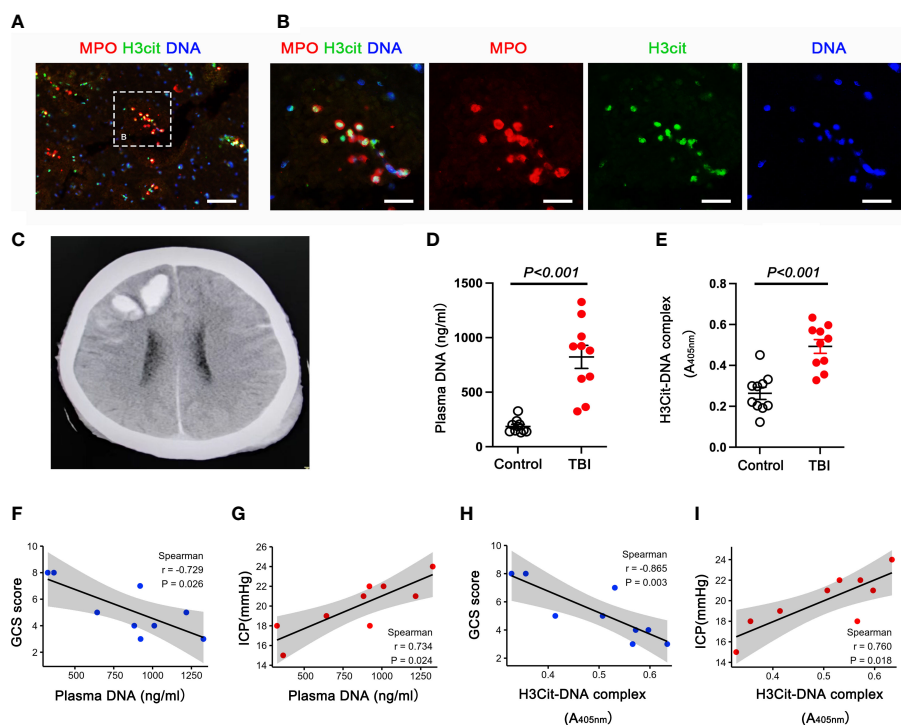


FIGURE 1

NETs are found in the brain and circulating blood from TBI patients and have a significant correlation with GCS and ICP. (A, B) Representative immunofluorescence images (A) displaying the NET formation (H3Cit-positive neutrophils) in the brain tissue sections from TBI patients. Enlarged images on the right side (B). Scale bar = 50 μ m (A); Scale bar = 200 μ m (B). A representative CT image from a TBI patient (C). The image shows the right frontal contusion and hematoma. (D, E) Quantification of the Levels of plasma DNA (D), plasma H3Cit-DNA complex (E) in the peripheral blood from healthy donors ($n = 10$) and TBI patients ($n = 10$). (F-I) Correlation among the levels of plasma DNA, plasma H3Cit-DNA complex with Glasgow Coma Scale (GCS) and intracranial pressure (ICP). Spearman correlation analysis was applied with $r = -0.729$, $P = 0.026$ (F) (plasma DNA correlate with GCS score), $r = 0.734$, $P = 0.024$ (G) (plasma DNA correlate with ICP), $r = -0.865$, $P = 0.003$ (H) (plasma H3Cit-DNA complex correlate with GCS score), $r = 0.734$, $P = 0.024$ (I) (plasma H3Cit-DNA complex correlate with ICP). The statistical graph shows that the higher the level of NETs, the greater the degree of TBI.

significantly elevated in TBI patients compared with matched healthy donors. Notably, a significant inverse correlation was observed between plasma DNA levels and GCS score, and a significant positive correlation was detected between plasma DNA levels and ICP (Figures 1F, G). Similarly, plasma H3Cit-DNA complex levels positively correlated with ICP, whereas inversely correlated with the GCS score. (Figures 1H, I). These results raise the unexplored possibility that NETs contribute to neurological deficits and cerebral edema after TBI.

Neutrophil infiltration and NETs formation in brain tissues are around the trauma area in mice with TBI

To verify the presence of neutrophil infiltration and NETs formation in the brain tissue of 3d mice after TBI. Double immunofluorescence staining of Ly6G and NETs-specific markers (citrullinated histone H3, H3cit), neutrophil, and neutrophil-derived NETs could be simply observed in the mouse brain sections after TBI (Figure 2A). It has been confirmed that the peak of neutrophil infiltration in mouse brain tissue is 3 days after TBI (42). Western Blot results that the protein expression of MPO, PAD4, and H3Cit was significantly increased in the cortex around the trauma area 3d post-TBI (Figures 2B–E).

Neutrophil depletion ameliorates neuronal function and neuronal death induced by NLRP1 after TBI

The rotary test and mNSS were used to assess neurological function in the acute phase after TBI. we found that anti-Ly6G treatment effectively improved neurological deficits in mice at 3 d after TBI (Figures 3A, B). Hematoxylin and eosin staining and Nissl staining showed massive degeneration and necrosis of neuronal cells 3 days after TBI. However, the number of neuronal deaths was significantly reduced in anti-Ly6G-treated mice compared with the vehicle group (Figures 3C–E). Additionally, we observed neuronal death by immunofluorescence staining of NEUN (red) and TUNEL (green) in the different groups (Figures 3F, G). The results showed that neuronal death was significantly reduced in the anti-Ly6G treatment group compared with the TBI+ vehicle group. NLRP1 (nucleotide-binding domain leucine-rich repeat pyrin domain containing 1) inflammasomes are primarily expressed in neurons and is closely related to neuronal pyroptosis. The results observed that the number of NLRP1 positive neurons in the anti-Ly6G treatment group was significantly reduced compared with the vehicle group (Figures 3H, I). Therefore, neutrophil infiltration was closely related to NLRP1-mediated neuronal pyroptosis after TBI by double immunofluorescence staining of NEUN (red) and NLRP1(green).

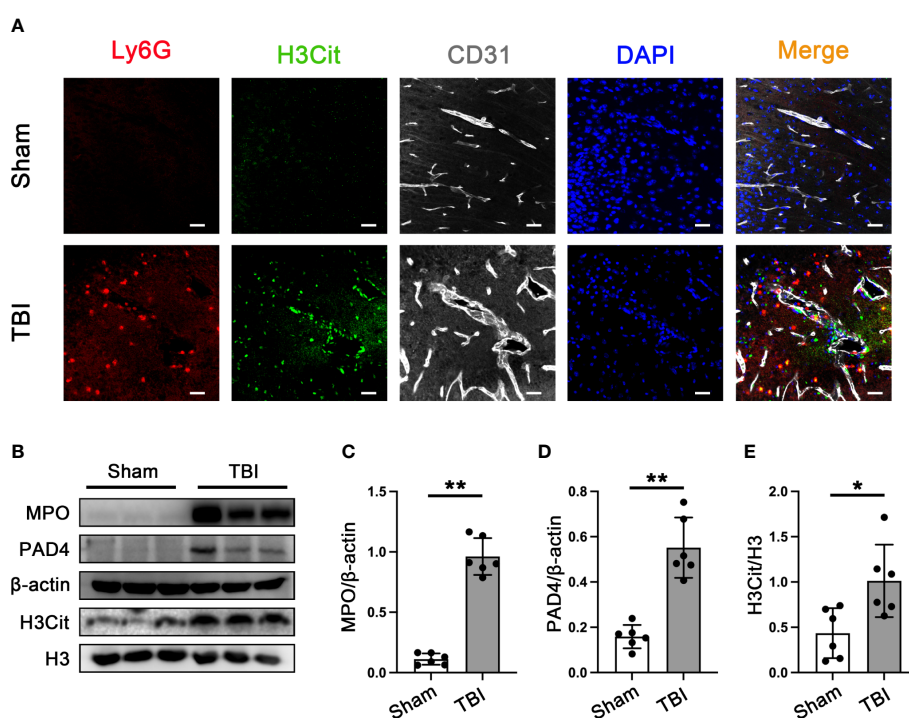


FIGURE 2

Neutrophils infiltration and NETs formation in mice brain tissue. (A) Representative immunofluorescence staining of Ly6G-positive neutrophils (red) and H3Cit -positive (green) and CD31-labeled blood vessels (white) in the mice brain tissue sections post-CCT 3 days. Nuclei were stained with DAPI (blue). (B) Representative Western blot bands of MPO, PAD4, H3Cit, and H3 and statistical analysis expression level of MPO (C), PAD4 (D), and H3Cit (E) in mice brain tissue (n=6). Data are represented as mean \pm SD. *P < 0.05, **P < 0.01.

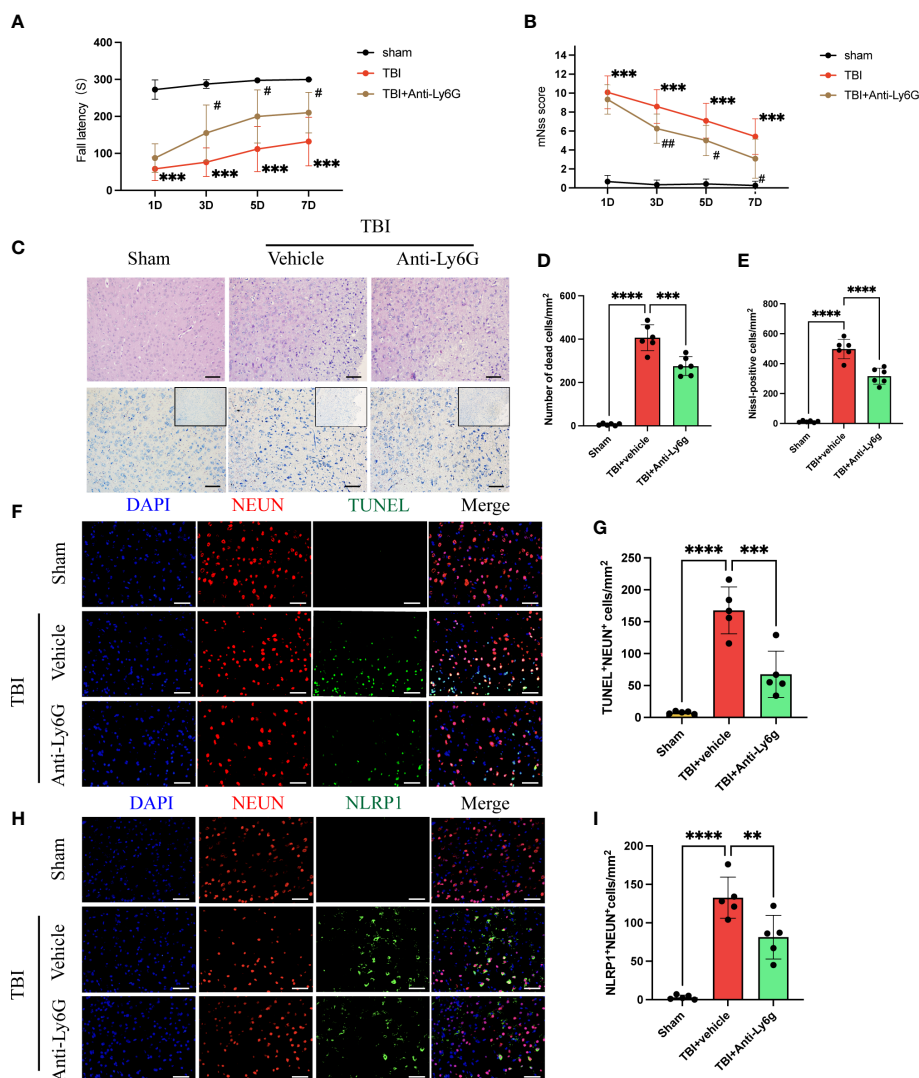


FIGURE 3

Neutrophil depletion ameliorates neurological function and reduces NLRP1-induced neuronal death after TBI. Rotary test (A) and modified neural severity scores (mNSS, B) were used to evaluate the neural function of mice treated with vehicle and Anti-Ly6G compared with the Sham group at 1 d, 3 d, 5 d, 7 d after TBI ($n = 12$). (C) Hematoxylin and eosin staining and Nissl staining of the cortex around the traumatic area 3 days after TBI ($n = 6$). Count the number of dead cells of Hematoxylin and eosin staining (D) and Nissl staining (E). Scale bar = 100 μm . (F) Representative immunofluorescence images of TUNEL-positive (green) cells and NEUN-positive (red) neurons in the peritraumatic cortex ($n = 6$). Count and compare the number of TUNEL-positive neurons in different groups (G). (H) Representative immunofluorescence images of NLRP1-positive (green) cells and NEUN-positive (red) neurons. Count and compare the number of NLRP1-positive neurons in different groups (I). Nuclei were stained with DAPI (blue). Scale bar = 100 μm . Data are represented as mean \pm SD. ** $P < 0.01$, *** $P < 0.001$ and **** $P < 0.0001$, compared within two groups. # $p < 0.05$, ## $p < 0.01$ and vs vehicle group.

Degradation of NETs-associated DNA ameliorates neuronal pyroptosis by inhibiting the STING- IRE1 α -NLRP1 pathway after TBI

We next confirm whether the degradation of NET-associated DNA with DNase 1 could ameliorate neuronal pyroptosis by inhibiting the STING-IRE1 α -NLRP1 pathway. Immunofluorescence staining showed the number of TUNEL-positive neurons remarkably increased in the cortex around the trauma area of TBI mice compared with the sham group (Figures 4A, B). In TBI mice treated with Dnase 1 the number of TUNEL-positive neurons significantly reduced in the

peripheral cortex of the trauma area (Figures 4A, B). Phosphorylated STING is an activated form of STING. In order to verify the activation of STING in neurons after TBI, immunofluorescence staining was used to observe the expression of P-STING in neurons (Supplementary Figure 1). The results showed that the expression of P-STING increased significantly in neurons after TBI, and DNase1 treatment could reverse this result. This effect of DNase 1 was abolished in mice that also received the second messenger cGAMP 3 d after TBI (Figures 4A, B). Consistent with this result, compared with TBI +vehicle group, DNase 1 treatment could significantly reduce the number of STING-positive neurons. However, cGAMP treatment can reverse the treatment advantage of DNase 1 (Figures 4A, C). Meanwhile, the number of

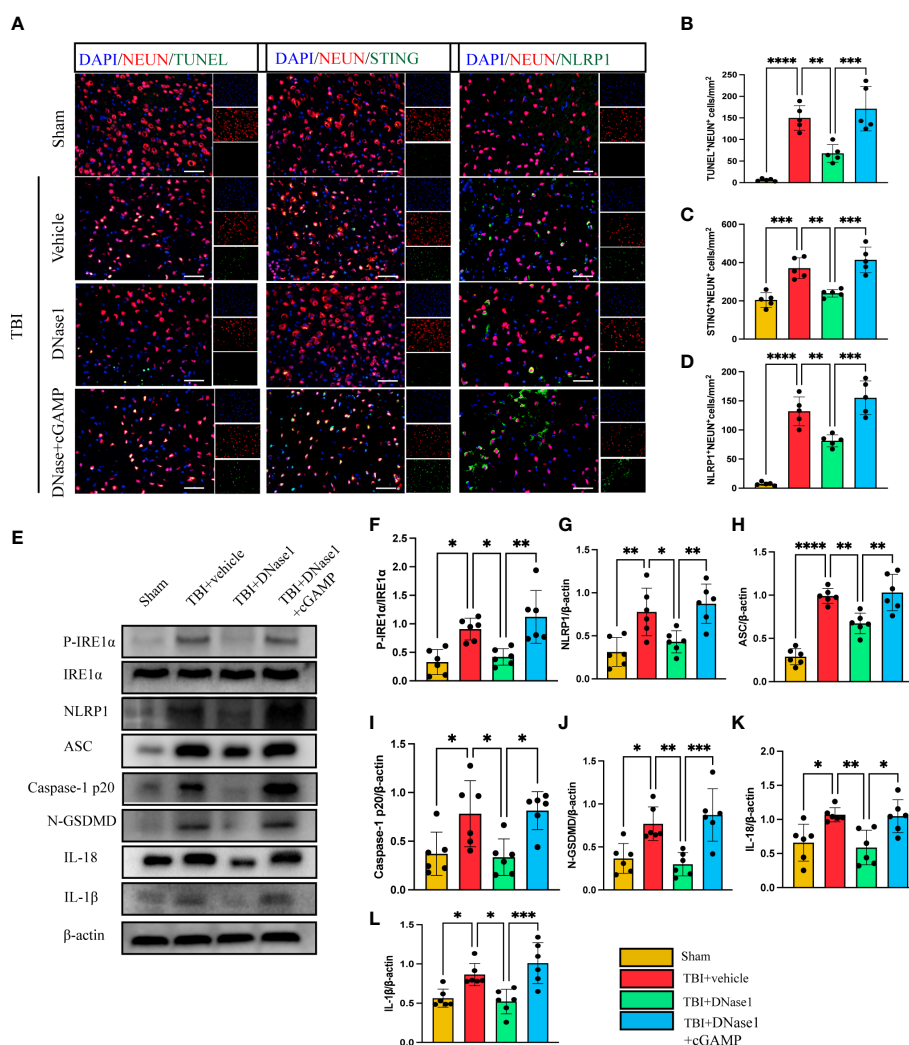


FIGURE 4

DNase 1 ameliorates neurons' pyroptosis by inhibiting the STING-IRE1 α -NLRP1 pathway after TBI. (A) Representative fluorescent double stain images of NEUN-positive neurons with TUNEL-positive cells (green), STING-positive cells (green) and NLRP1-positive cells (green) in the peritraumatic cortex (n=5). Nuclei were stained with DAPI (blue). Scale bar = 50 μ m. Count and analyze the number of double-stained positive cells of NEUN-positive neurons with TUNEL-positive cells (B), STING-positive cells (C) and NLRP1-positive cells (D). (E) Representative Western blot bands of P-IRE1 α , NLRP1, ASC, Caspase-1 p20, N-GSDMD, IL-18, IL-1 β and statistical analysis expression level of P-IRE1 α (F), NLRP1 (G), ASC (H), Caspase-1 p20 (I), N-GSDMD (J), IL-18 (K), IL-1 β (L) in brain tissue of mice post-TBI 3 days (n=6). Data are presented as mean \pm SD. *P < 0.05, **P < 0.01, ***P < 0.001 and ****P < 0.0001.

NLRP1-positive neurons was significantly reduced in DNase 1 treatment mice with TBI. Interestingly, cGAMP treatment also reversed the therapeutic effects of DNase 1 (Figures 4A, D). Therefore, STING can activate the pyroptosis pathway of neurons. We subsequently found that the protein expression of P-IRE1 α , NLRP1, ASC, Caspase-1 p20, N-GSDMD, IL-18, and IL-1 β were remarkably upregulated in the cortex of mice subjected to TBI (Figures 4E-L). DNase 1 treatment significantly rescued the activation of the STING-IRE1 α -NLRP1 pathway and reduced protein products associated with neuronal pyroptosis. However, treatment with the cGAMP effectively reversed the effect of DNase 1 on the STING-IRE1 α -NLRP1 pathway (Figures 4E-L). These results showed that degradation of neutrophil-released NETs associated DNA with DNase 1 could rescue neuronal pyroptosis by inhibiting the STING-IRE1 α -NLRP1 pathway.

Inhibition of PAD4 ameliorates neurological function and neuronal pyroptosis by inhibiting the STING/IRE1 α -NLRP1 pathway after TBI

Peptidylarginine deiminase 4 (PAD4) catalyzes histone citrullination that plays a key role in NETs formation (43, 44). We examined a hypothesis on whether inhibition of PAD4 (CL-amidine) to reduce NETs-formation improved neural function and reduced neuronal pyroptosis. First, Nissl staining showed that the number of neuronal deaths was significantly reduced in CL-amidine treatment mice compared with the vehicle group (Figures 5A, B). However, treatment with cGAMP could reverse the effectiveness of CL-amidine after TBI (Figures 5A, B). First, confocal microscopy was used to observe the brain tissue stained by immunofluorescence, and it was

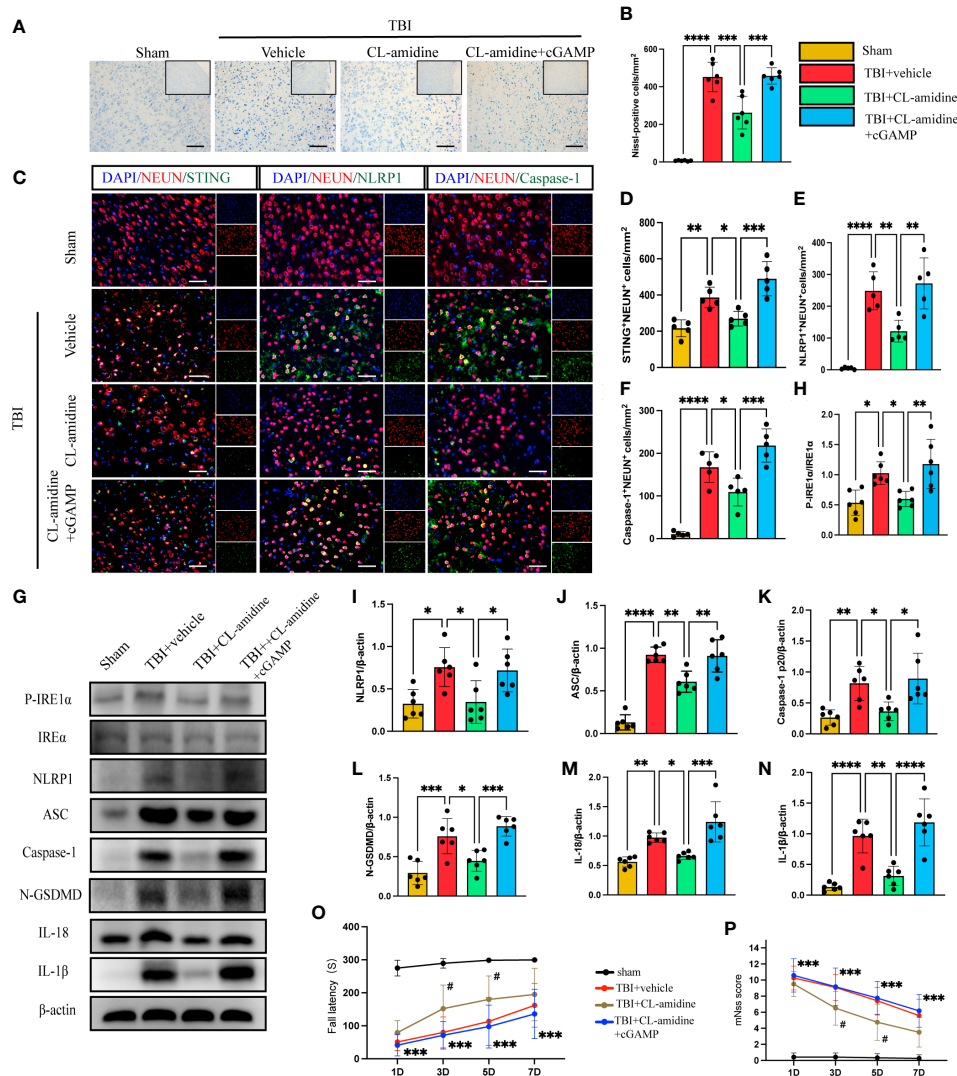


FIGURE 5

Inhibition of PAD4 ameliorates neurons' pyroptosis by inhibiting the STING-IRE1 α -NLRP1 pathway. (A) Nissl staining images of the peri-injured brain tissue of mice. Count the number of Nissl-positive cells in the different groups (B). Scale bar = 100 μ m. (C) Representative fluorescent double stain images of NEUN-positive neurons with STING-positive cells (green) and Caspase-1-positive cells (green) in the peritraumatic cortex (n=5). Nuclei were stained with DAPI (blue). Scale bar = 50 μ m. Count and analyze the number of double-stained positive cells of NEUN-positive neurons with STING-positive cells (D), NLRP1-positive cells (E) and Caspase-1-positive cells (F) in the different groups. (G) Representative Western blot bands of P-IRE1 α , NLRP1, ASC, Caspase-1 p20, N-GSDMD, IL-18, IL-1 β and statistical analysis expression level of P-IRE1 α (H), NLRP1 (I), ASC (J), Caspase-1 p20 (K), N-GSDMD (L), IL-18 (M), IL-1 β (N) in brain tissue of mice post-TBI 3 days (n=6). Rotary test (O) and mNSS (P) were used to evaluate the neural function of mice treated with PBS and Anti-Ly6G compared with the Sham group at 1 d, 3 d, 5 d, 7d after TBI (n = 12). Scale bar = 50 μ m. Data are presented as mean \pm SD. *P < 0.05, **P < 0.01, ***P < 0.001 and ****P < 0.0001 compared within two groups. #p < 0.05 and vs CL-amidine+ cGAMP group.

found that STING/NLRP1 and STING/Caspase-1 could be expressed simultaneously in the same neuron (Supplementary Figure 2). In addition, immunofluorescence staining showed that treatment with CL-amidine significantly reduced the number of STING-positive, NLRP1-positive, and Caspase-1-positive neurons in the cortex surrounding the trauma area (Figures 5C–F). On the contrary, cGAMP treatment could block the effectiveness of CL-amidine (Figures 5C–F). The protein levels of P- IRE1 α , NLRP1, ASC, Caspase-1 p20, N-GSDMD, IL-18, and IL-1 β were detected by western blot and it was found that the protein expression level of STING/P- IRE1 α -NLRP1 pathway and neuronal pyroptosis-related

protein products in the CL-amidine treatment group were significantly down-regulated compared with TBI+ vehicle group (Figures 5G–N). However, the protein level of the STING-IRE1 α -NLRP1 pathway and neuronal pyroptosis-related protein products were still up-regulated in the mice that interfered with both CL-amidine and cGAMP (Figures 5G–N). Meanwhile, the results of the rotary test and mNSS scores showed that Inhibition of PAD4 could remarkably ameliorate neurological deficits of mice on day 3 after TBI (Figures 5O, P). These results showed that Inhibition of PAD4 could ameliorate neurological deficits and recuse neuronal pyroptosis by inhibiting the STING-IRE1 α -NLRP1 pathway.

Activated PAD4 promotes neuronal pyroptosis through the STING-IRE1 α -NLRP1 pathway after TBI

To study whether that increased formation of NET, orchestrated by PAD4, contributed to neuronal pyroptosis, we first studied the role of overexpression of PAD4 on neuronal pyroptosis in mice with TBI. Immunofluorescence staining showed extensive expression of recombinant adeno-PAD4-EGFP-infected cells in the cortex 3 d after injection (Supplementary Figure 3). It can be seen from the figure that the expression of PAD4 is mainly concentrated in neutrophils. Immunofluorescence staining showed that administration of PAD4 adenovirus into the cortex led to a remarkable increase in the number of neuronal death (TUNEL-positive neurons), STING-positive neurons, and NLRP1-

positive neurons (Figures 6A–D). Interestingly, STING inhibitor C176 could block the function of PAD4 adenovirus (Figures 6A–D). Meanwhile, the protein expression level of the STING- P- IRE1 α -NLRP1 pathway and neuronal pyroptosis-related protein products were also detected by Western Blot. The results indicated that the protein levels of P- IRE1 α , NLRP1, ASC, Caspase-1 p20, N- GSDMD, and IL-18 were significantly increased after the administration of PAD4 adenovirus into the cortex (Figures 6E–K). However, STING inhibitor C-176 could decrease the expression level of related proteins after TBI and reverse the effect of PAD4 adenovirus (Figures 6E–K). Finally, we evaluated neurological function during the acute phase post-TBI by rotary test and mNSS scores after administration of PAD4 adenovirus and PAD4 adenovirus + C176. The results showed that the PAD4 adenovirus group aggravated nerve damage after TBI, and C176 improved the

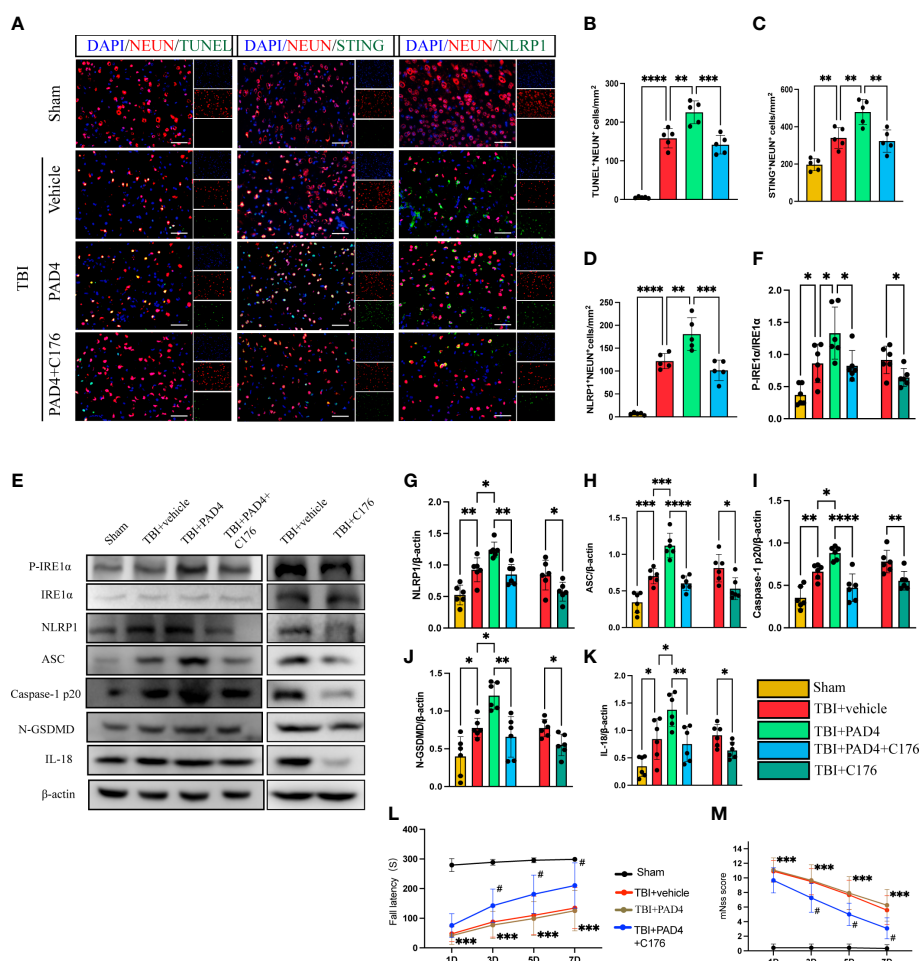


FIGURE 6

Overexpression of PAD4 exacerbates neurons' pyroptosis by promoting the STING-IRE1 α -NLRP1 pathway. (A) Representative fluorescent double stain images of NEUN-positive neurons with TUNEL-positive cells (green), STING-positive cells (green) and NLRP1-positive cells (green) in the peritraumatic cortex (n=5). Nuclei were stained with DAPI (blue). Scale bar = 50 μ m. Count and analyze the number of double-stained positive cells of NEUN-positive neurons with TUNEL-positive cells (B), STING-positive cells (C) and NLRP1-positive cells (D). (E) Representative Western blot bands of P-IRE1 α , NLRP1, ASC, Caspase-1 p20, N-GSDMD, IL-18 and statistical analysis expression level of P-IRE1 α (F), NLRP1 (G), ASC (H), Caspase-1 p20 (I), N-GSDMD (J) and IL-18 (K) in brain tissue of mice post-TBI 3 days (n=6). Rotary test (L) and mNSS (M) were used to evaluate the neural function of mice treated with PBS and Anti-Ly6G compared with the Sham group at 1 d, 3 d, 5 d, 7d after TBI (n = 12). Data are presented as mean \pm SD. *P < 0.05, **P < 0.01, ***P < 0.001 and ****P < 0.0001 compared within two groups. #p < 0.05 and vs PAD4+C176 group.

adverse effects caused by PAD4 adenovirus (Figures 6L, M). These results showed PAD4 played a key role in NLRP1-induced neuronal pyroptosis *via* STING/IRE1 α pathway.

Inhibition of IRE1 α improves through the STING-IRE1 α -NLRP1 pathway after TBI

To explore whether IRE1 α is a key part of the pathway that NETs cause neuronal pyroptosis. We used IRE inhibitor Kira6 after the administration of PAD4 adenovirus into the cortex to observe the expression of pathway proteins. The results found that the protein expression of P-IRE1 α was significantly increased in the PAD4 adenovirus group and IRE inhibitor Kira6 could block the effect of PAD4 adenovirus (Figures 7A, B). Meanwhile, Immunoblotting showed the protein expression of NLRP1, ASC, Caspase-1 p20, N-GSDMD, and IL-18 were significantly reduced after the administration of Kira6 compared with the DMSO group and the PAD4 adenovirus group. (Figures 7A, C–G). These data suggest that IRE1 α plays a key role in NLRP1-induced neuronal pyroptosis by promoting NETs formation.

Discussion

In the present study, we first confirmed the increased infiltration of NETs in the contused brain of TBI patients. Furthermore, we found that increased markers of NET formation in the circulation plasma of TBI patients correlate with elevated intracranial pressure (ICP) and worse neurological function. Moreover, we found that neutrophils and NET formation in the cortex parenchyma is increased in mice subjected to TBI, and depletion of neutrophils with Anti-Ly6G effectively reduced NET formation and ameliorated neurological deficits and attenuated NLRP1-mediated neuronal cell pyroptosis. In addition, we demonstrated that the degradation of NETs or inhibition of NET formation attenuated NLRP1-mediated neuronal cell pyroptosis in a STING-dependent way. Notably, after overexpression of NET formation by adenoviruses in TBI mice, the NLRP1-mediated neuronal cell pyroptosis increased, whereas this effect was effectively abolished by a STING inhibitor. Another novel finding of the current study is that NETs can activate STING-dependent ER stress and IRE1 α inhibitor effectively attenuates NETs-induced neuronal pyroptotic death after TBI. Collectively, NET formation

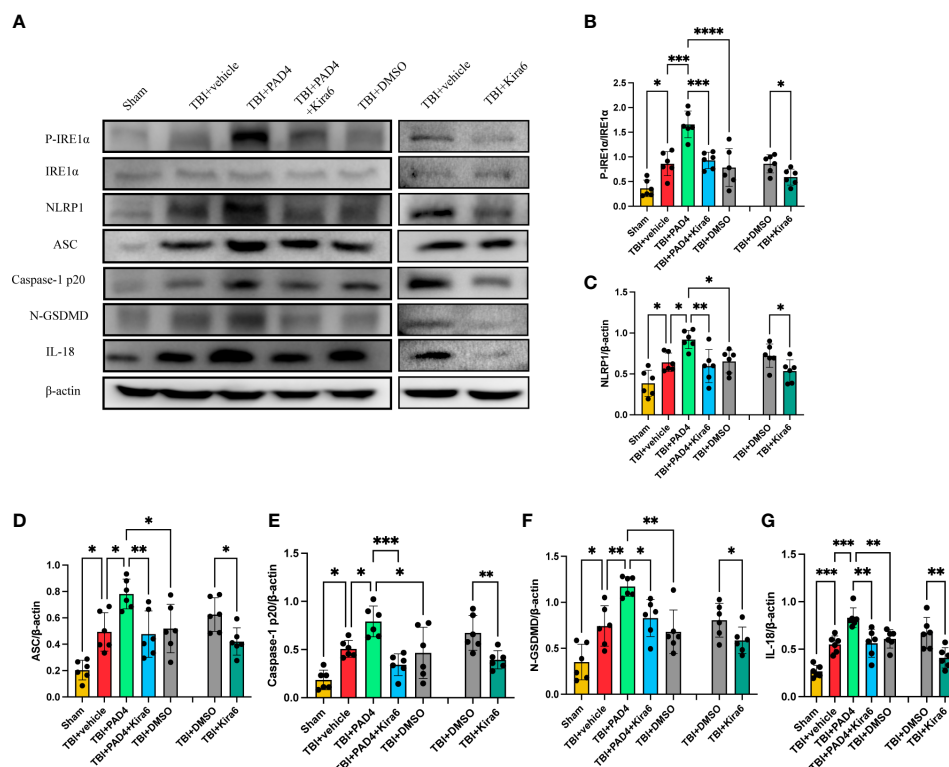


FIGURE 7

Inhibition of IRE1 α ameliorates neurons' pyroptosis by inhibiting the STING-IRE1 α -NLRP1 pathway. (A) Representative Western blot bands of P-IRE1 α (B), NLRP1 (C), ASC (D), Caspase-1 p20 (E), N-GSDMD (F) and IL-18 (G), and statistical analysis expression level of STING (B), P-IRE1 α (B), NLRP1 (C), ASC (D), Caspase-1 p20 (E), N-GSDMD (F) and IL-18 (G) in brain tissue of mice post-TBI 3 days (n=6). Data are presented as mean \pm SD. *P < 0.05, **P < 0.01, ***P < 0.001 and ****P < 0.0001 compared within two groups.

promotes NLRP1 inflammasome-mediated neuronal pyroptosis after TBI, at least partly through STING/IRE1 α signaling pathway.

Pathologically, programmed neuronal cell death and secondary inflammation are two common hallmarks of TBI (45). Programmed neuronal cell death is characterized by any form of cell death caused by either an intracellular or extracellular death program, including apoptosis, necroptosis, autophagy, and pyroptosis (45). Intriguingly, unlike any other programmed cell death, pyroptosis is a highly inflammatory form of programmed cell death mediated by cleaved caspase-1 and/or caspase-11 (46). Previous studies demonstrated that NLRP1 inflammasomes are primarily expressed in neurons (9), and NLRP1 inflammasomes modulate caspase-1 cleavage and consequent IL-1 β and IL-18 processing (47). In a rat model of spinal cord injury, the mRNA and protein of NLRP1 were significantly elevated from 18 to 24 hours after spinal cord injury (48). A previous study showed that silencing NLRP1 inflammasome reduced neuronal cell pyroptosis in a mouse model of Alzheimer's disease (49). Importantly, emerging evidence also demonstrated that NLRP1 inflammasome activation promotes neuronal cell pyroptosis and neurological deficits after brain injury (5, 30, 47, 50). Similarly, we observed that the expression of NLRP1 was significantly upregulated and inhibition of the STING/IRE1 α signaling pathway effectively rescued NLRP1-dependent neuronal pyroptosis and secondary neuronal apoptosis in mice subjected to TBI.

NETs are lattices of extracellular DNA, released by neutrophils meant to trap and kill pathogens. However, there is increasing evidence to suggest that dysfunction of the NET inhibition mechanism and excessive NET production are also important pathogenic mechanisms that may lead to various diseases (51). A recent study also revealed that excessive NETs can lead to neurological deficits, brain edema, and microcirculatory dysfunction after experimental TBI (13). Circulating NETs biomarkers have been reported to be associated with elevated ICP and worse neurological function in TBI patients (13). Similar results were also detected in our research, in which peripheral plasma NETs, both ds-DNA, and the H3Cit-DNA complex were significantly elevated in TBI patients. Moreover, we also found that neutrophils-derived NETs were significantly increased in brain tissue from TBI patients. Importantly, circulating NETs significantly correlated significantly with elevated ICP and worse neurological function in TBI patients. However, the contribution of NETs to TBI-induced neuronal pyroptotic death and neurological deficits remains to be elucidated. A previous study demonstrated that NET formation was upregulated in brain parenchyma in mice subjected to ischemic stroke and NETs as the main source circulating ds-DNA, could contribute to neuroinflammation and blood-brain barrier disruption *via* the cGAS/STING pathway (33, 37). Notably, STING has been reported to be primarily expressed in neurons and microglia in the brain (52). Consistently, our research found that STING-positive neurons were significantly increased in mice subjected to TBI. In addition, further investigation in our research revealed that degradation of NETs or inhibition of NET formation significantly inhibited STING upregulation in neurons and attenuated neuronal pyroptosis after TBI, whereas overexpression of peptidylarginine deiminase 4 [a key enzyme of

NET formation (53)] in the cortex following stereotactic adenoviruses injection could aggravate STING-dependent neuronal pyroptosis. Collectively, these results confirmed that NETs play a detrimental role in promoting neuronal pyroptosis *via* the NETs- STING pathway after TBI.

Severe ER stress is associated with multiple pathophysiological processes of TBI including neuroinflammation, neuronal cell death, blood-brain barrier damage, axon injury, neurodegeneration, etc (45). IRE1 α , as one of the vital ER stress sensors, was found to play a critical role in neuronal death, especially in NLRP1 inflammasome-mediated neuronal pyroptosis (30). Consistently, in current experimental research, we found that IRE1 α activation was significantly enhanced following TBI, and inhibition of IRE1 α effectively rescued NLRP1 inflammasome-mediated neuronal pyroptosis. A recent study reported that NETs could promote intestinal epithelial cell death by regulating ER stress activation-associated protein kinase RNA-like ER kinase (PERK) signaling pathways (31). However, whether and how the NET formation is related to IRE1 α activation remains unclear. In the present study, we found that degradation of NETs or inhibition of NET formation significantly inhibited IRE1 α activation-associated neuronal pyroptosis after TBI, whereas, overexpression of NETs effectively aggravated IRE1 α activation and neuronal death. Importantly, we also explained why NET formation is associated with the activation of IRE1 α in the present research. STING, a transmembrane protein located on the endoplasmic reticulum (ER), was demonstrated to act as a bridge between the NETs and IRE1 α in our current research.

Several limitations of this study need to be discussed here. First, we did not evaluate the effects of NETs on neural pyroptosis in different age groups or TBI with systemic comorbidities and female animals. Further studies are needed to certify the effect of NETs on neurons in experimental TBI in different age groups and females. Then, in the sample of TBI patients, there was no assessment of the influence of the patient's operation time and operation area on the experimental results. In addition, in this study, cGAMP, as a product of cGAS, was used as the activator of STING to confirm the role of STING in neurons. However, the role of the cGAS-STING pathway in neuronal pyroptosis caused by NETs is not much confirmed. Further studies are needed to investigate the specific role of cGAS in NETs-mediated STING pathway activation in neurons.

Conclusions

Our study revealed that NETs were involved in TBI-induced neuronal pyroptosis. It was verified again that the increased NET formation was associated with elevated ICP and worse neurological function in TBI patients. Degradation of NETs or inhibition of NET formation with PAD inhibitor ameliorated TBI-induced IRE1 α activation and NLRP1 inflammasome-mediated neuronal pyroptosis, whereas overexpression of NET formation aggravated neuronal pyroptotic death and neurological dysfunction. Moreover, the STING antagonist effectively rescued IRE1 α activation and NLRP1 inflammasome-mediated neuronal pyroptosis after TBI. Importantly,

the IRE1 α antagonist also inhibited NET-induced neuronal pyroptosis and neurological deficits. Collectively, these findings indicated that suppression of the NETs-STING-IRE1 α pathway may be protective in TBI-induced NLRP1 inflammasome-mediated neuronal pyroptosis and neurological deficits.

Data availability statement

The original contributions presented in the study are included in the article/**Supplementary Material**. Further inquiries can be directed to the corresponding authors.

Ethics statement

The animal study was reviewed and approved by National Institutes of Health Guide for the Care and Use of Laboratory Animals and approved by Tianjin Medical University Animal Care and Use committee. Written informed consent was obtained from the individual(s) for the publication of any potentially identifiable images or data included in this article.

Author contributions

XC, SZ, JZ designed the experiment. YC MS, LL, XM, and HJ performed most of the experiments. XL, ZC, YuZ, SL, GY assisted in data analysis. QD, FC, XC wrote the manuscript. YaZ supplements the data. SZ, JZ provided the overall guidance. All authors contributed to the article and approved the submitted version.

Funding

This work was supported by grants from the National Natural Science Foundation of China (no. 81930031, 81901525, 81801234,

and 82071389), the Natural Science Foundation of Tianjin (No.19JCQNJC09500), the Science & Technology Development Fund of Tianjin Education Commission for Higher Education (No. 2019ZD034) and the Science & Technology Development Fund of Tianjin (NO.22JRRRCRC00020).

Acknowledgments

The authors are grateful to Ying Li, Lei Zhou, Hao Liang, Weiyun Cui and Li Liu from the Tianjin Neurological Institute for providing technical support.

Conflict of interest

The authors declare that the research was conducted in the absence of any commercial or financial relationships that could be construed as a potential conflict of interest.

Publisher's note

All claims expressed in this article are solely those of the authors and do not necessarily represent those of their affiliated organizations, or those of the publisher, the editors and the reviewers. Any product that may be evaluated in this article, or claim that may be made by its manufacturer, is not guaranteed or endorsed by the publisher.

Supplementary material

The Supplementary Material for this article can be found online at: <https://www.frontiersin.org/articles/10.3389/fimmu.2023.1125759/full#supplementary-material>

References

1. Collaborators GBDN. Global, regional, and national burden of neurological disorders, 1990-2016: a systematic analysis for the global burden of disease study 2016. *Lancet Neurol* (2019) 18:459–80. doi: 10.1016/S1474-4422(18)30499-X
2. Stocchetti N, Carbonara M, Citerio G, Ercole A, Skrifvars MB, Smielewski P, et al. Severe traumatic brain injury: targeted management in the intensive care unit. *Lancet Neurol* (2017) 16:452–64. doi: 10.1016/S1474-4422(17)30118-7
3. Jassam YN, Izzy S, Whalen M, McGavern DB, El Khoury J. Neuroimmunology of traumatic brain injury: Time for a paradigm shift. *Neuron* (2017) 95:1246–65. doi: 10.1016/j.neuron.2017.07.010
4. Fann DY, Lee SY, Manzanero S, Tang SC, Gelderblom M, Chunduri P, et al. Intravenous immunoglobulin suppresses NLRP1 and NLRP3 inflammasome-mediated neuronal death in ischemic stroke. *Cell Death Dis* (2013) 4:e790. doi: 10.1038/cddis.2013.326
5. Yan J, Xu W, Lenahan C, Huang L, Wen J, Li G, et al. CCR5 activation promotes NLRP1-dependent neuronal pyroptosis via CCR5/PKA/CREB pathway after intracerebral hemorrhage. *Stroke* (2021) 52:4021–32. doi: 10.1161/STROKEAHA.120.033285
6. Shi J, Gao W, Shao F. Pyroptosis: Gasdermin-mediated programmed necrotic cell death. *Trends Biochem Sci* (2017) 42:245–54. doi: 10.1016/j.tibs.2016.10.004
7. de Rivero Vaccari JP, Dietrich WD, Keane RW. Activation and regulation of cellular inflammasomes: gaps in our knowledge for central nervous system injury. *J Cereb Blood Flow Metab* (2014) 34:369–75. doi: 10.1038/jcbfm.2013.227
8. Guo H, Callaway JB, Ting JP. Inflammasomes: mechanism of action, role in disease, and therapeutics. *Nat Med* (2015) 21:677–87. doi: 10.1038/nm.3893
9. Yap JKY, Pickard BS, Chan EWL, Gan SY. The role of neuronal NLRP1 inflammasome in alzheimer's disease: Bringing neurons into the neuroinflammation game. *Mol Neurobiol* (2019) 56:7741–53. doi: 10.1007/s12035-019-1638-7
10. Liu W, Chen Y, Meng J, Wu M, Bi F, Chang C, et al. Ablation of caspase-1 protects against TBI-induced pyroptosis *in vitro* and *in vivo*. *J Neuroinflamm* (2018) 15:48. doi: 10.1186/s12974-018-1083-y
11. Bi F, Ma H, Ji C, Chang C, Liu W, Xie K. Rhein protects against neurological deficits after traumatic brain injury in mice *via* inhibiting neuronal pyroptosis. *Front Pharmacol* (2020) 11:564367. doi: 10.3389/fphar.2020.564367
12. Ismael S, Nasoohi S, Ishrat T. MCC950, the selective inhibitor of nucleotide oligomerization domain-like receptor protein-3 inflammasome, protects mice against traumatic brain injury. *J Neurotrauma* (2018) 35:1294–303. doi: 10.1089/neu.2017.5344

13. Vaibhav K, Braun M, Alverson K, Khodadadi H, Kutiyawalla A, Ward A, et al. Neutrophil extracellular traps exacerbate neurological deficits after traumatic brain injury. *Sci Adv* (2020) 6:eax8847. doi: 10.1126/sciadv.aax8847
14. Papayannopoulos V. Neutrophil extracellular traps in immunity and disease. *Nat Rev Immunol* (2018) 18:134–47. doi: 10.1038/nri.2017.105
15. Sorvillo N, Cherpokova D, Martinod K, Wagner DD. Extracellular DNA NET-works with dire consequences for health. *Circ Res* (2019) 125:470–88. doi: 10.1161/CIRCRESAHA.119.314584
16. Kaplan MJ, Radic M. Neutrophil extracellular traps: double-edged swords of innate immunity. *J Immunol* (2012) 189:2689–95. doi: 10.4049/jimmunol.1201719
17. Schauer C, Janko C, Munoz LE, Zhao Y, Kienhofer D, Frey B, et al. Aggregated neutrophil extracellular traps limit inflammation by degrading cytokines and chemokines. *Nat Med* (2014) 20:511–7. doi: 10.1038/nm.3547
18. Dwivedi N, Radic M. Citrullination of autoantigens implicates NETosis in the induction of autoimmunity. *Ann Rheum Dis* (2014) 73:483–91. doi: 10.1136/annrheumdis-2013-203844
19. Sharma S, Hofbauer TM, Ondracek AS, Chausheva S, Alimohammadi A, Artner T, et al. Neutrophil extracellular traps promote fibrous vascular occlusions in chronic thrombosis. *Blood* (2021) 137:1104–16. doi: 10.1182/blood.2020005861
20. Denorme F, Portier E, Rustad JL, Cody MJ, de Araujo CV, Hoki C, et al. Neutrophil extracellular traps regulate ischemic stroke brain injury. *J Clin Invest* (2022) 132(10):e154225. doi: 10.1172/JCI154225
21. Laridan E, Denorme F, Desender L, Francois O, Andersson T, Deckmyn H, et al. Neutrophil extracellular traps in ischemic stroke thrombi. *Ann Neurol* (2017) 82:223–32. doi: 10.1002/ana.24993
22. Chen Y, Zhang H, Hu X, Cai W, Ni W, Zhou K. Role of NETosis in central nervous system injury. *Oxid Med Cell Longev* (2022) 2022:3235524. doi: 10.1155/2022/3235524
23. Hartlova A, Erttmann SF, Raffi FA, Schmalz AM, Resch U, Anugula S, et al. DNA Damage primes the type I interferon system via the cytosolic DNA sensor STING to promote anti-microbial innate immunity. *Immunity* (2015) 42:332–43. doi: 10.1016/j.immuni.2015.01.012
24. Apel F, Andreeva L, Knackstedt LS, Streeck R, Frese CK, Goosmann C, et al. The cytosolic DNA sensor cGAS recognizes neutrophil extracellular traps. *Sci Signal* (2021) 9:14(673):eaax7942. doi: 10.1126/scisignal.aax7942
25. Wu J, Chen YJ, Dobbs N, Sakai T, Liou J, Miner JJ, et al. STING-mediated disruption of calcium homeostasis chronically activates ER stress and primes T cell death. *J Exp Med* (2019) 216:867–83. doi: 10.1084/jem.20182192
26. Zhang Y, Chen W, Wang Y. STING is an essential regulator of heart inflammation and fibrosis in mice with pathological cardiac hypertrophy via endoplasmic reticulum (ER) stress. *BioMed Pharmacother* (2020) 125:110022. doi: 10.1016/j.biopha.2020.110022
27. Huang R, Shi Q, Zhang S, Lin H, Han C, Qian X, et al. Inhibition of the cGAS-STING pathway attenuates lung Ischemia/Reperfusion injury via regulating endoplasmic reticulum stress in alveolar epithelial type II cells of rats. *J Inflammation Res* (2022) 15:5103–19. doi: 10.2147/JIR.S365970
28. Abdullah A, Zhang M, Frugier T, Bedoui S, Taylor JM, Crack PJ. STING-mediated type-I interferons contribute to the neuroinflammatory process and detrimental effects following traumatic brain injury. *J Neuroinflamm* (2018) 15:323. doi: 10.1186/s12974-018-1354-7
29. Zhang LM, Xin Y, Wu ZY, Song RX, Miao HT, Zheng WC, et al. STING mediates neuroinflammatory response by activating NLRP3-related pyroptosis in severe traumatic brain injury. *J Neurochem* (2022) 162:444–62. doi: 10.1111/jnc.15678
30. Huang J, Lu W, Doycheva DM, Gamdzkyk M, Hu X, Liu R, et al. IRE1alpha inhibition attenuates neuronal pyroptosis via miR-125/NLRP1 pathway in a neonatal hypoxic-ischemic encephalopathy rat model. *J Neuroinflamm* (2020) 17:152. doi: 10.1186/s12974-020-01796-3
31. Sun S, Duan Z, Wang X, Chu C, Yang C, Chen F, et al. Neutrophil extracellular traps impair intestinal barrier functions in sepsis by regulating TLR9-mediated endoplasmic reticulum stress pathway. *Cell Death Dis* (2021) 12:606. doi: 10.1038/s41419-021-03896-1
32. Shi M, Mi L, Li F, Li Y, Zhou Y, Chen F, et al. Fluvoxamine confers neuroprotection via inhibiting infiltration of peripheral leukocytes and M1 polarization of Microglia/Macrophages in a mouse model of traumatic brain injury. *J Neurotrauma* (2022) 39:1240–61. doi: 10.1089/neu.2021.0355
33. Kang L, Yu H, Yang X, Zhu Y, Bai X, Wang R, et al. Neutrophil extracellular traps released by neutrophils impair revascularization and vascular remodeling after stroke. *Nat Commun* (2020) 11:2488. doi: 10.1038/s41467-020-16191-y
34. Zhai Y, Ye SY, Wang QS, Xiong RP, Fu SY, Du H, et al. Overexpressed ski efficiently promotes neurorestoration, increases neuronal regeneration, and reduces astrogliosis after traumatic brain injury. *Gene Ther* (2022). 30(1-2):2348 doi: 10.1038/s41434-022-00320-x
35. Wei P, Wang K, Luo C, Huang Y, Misilimu D, Wen H, et al. Cordycepin confers long-term neuroprotection via inhibiting neutrophil infiltration and neuroinflammation after traumatic brain injury. *J Neuroinflamm* (2021) 18:137. doi: 10.1186/s12974-021-02188-x
36. Ding R, Li H, Liu Y, Ou W, Zhang X, Chai H, et al. Activating cGAS-STING axis contributes to neuroinflammation in CVST mouse model and induces inflammasome activation and microglia pyroptosis. *J Neuroinflamm* (2022) 19:137. doi: 10.1186/s12974-022-02511-0
37. Wang R, Zhu Y, Liu Z, Chang L, Bai X, Kang L, et al. Neutrophil extracellular traps promote tPA-induced brain hemorrhage via cGAS in mice with stroke. *Blood* (2021) 138:91–103. doi: 10.1182/blood.2020008913
38. Chopra S, Giovanelli P, Alvarado-Vazquez PA, Alonso S, Song M, Sandoval TA, et al. IRE1alpha-XBP1 signaling in leukocytes controls prostaglandin biosynthesis and pain. *Science* (2019) 365(6450):eaau6499. doi: 10.1126/science.aau6499
39. Chen X, Chen C, Fan S, Wu S, Yang F, Fang Z, et al. Omega-3 polyunsaturated fatty acid attenuates the inflammatory response by modulating microglia polarization through SIRT1-mediated deacetylation of the HMGB1/NF-kappaB pathway following experimental traumatic brain injury. *J Neuroinflamm* (2018) 15:116. doi: 10.1186/s12974-018-1151-3
40. Hu J, Wang X, Chen X, Fang Y, Chen K, Peng W, et al. Hydroxychloroquine attenuates neuroinflammation following traumatic brain injury by regulating the TLR4/NF-kappaB signaling pathway. *J Neuroinflamm* (2022) 19:71. doi: 10.1186/s12974-022-02430-0
41. Shi M, Liu L, Min X, Mi L, Chai Y, Chen F, et al. Activation of sigma-1 receptor alleviates ER-associated cell death and microglia activation in traumatically injured mice. *J Clin Med* (2022) 22:11(9):2348. doi: 10.3390/jcm11092348
42. Szymdynger-Chodobska J, Strazielle N, Zink BJ, Ghersi-Egea JF, Chodobski A. The role of the choroid plexus in neutrophil invasion after traumatic brain injury. *J Cereb Blood Flow Metab* (2009) 29:1503–16. doi: 10.1038/jcbfm.2009.71
43. Martinod K, Demers M, Fuchs TA, Wong SL, Brill A, Gallant M, et al. Neutrophil histone modification by peptidylarginine deiminase 4 is critical for deep vein thrombosis in mice. *Proc Natl Acad Sci U.S.A.* (2013) 110:8674–9. doi: 10.1073/pnas.1301059110
44. Wang Y, Li M, Stadler S, Correll S, Li P, Wang D, et al. Histone hypercitrullination mediates chromatin decondensation and neutrophil extracellular trap formation. *J Cell Biol* (2009) 184:205–13. doi: 10.1083/jcb.200806072
45. Shi M, Chai Y, Zhang J, Chen X. Endoplasmic reticulum stress-associated neuronal death and innate immune response in neurological diseases. *Front Immunol* (2021) 12:794580. doi: 10.3389/fimmu.2021.794580
46. Datta A, Sarmah D, Mounica L, Kaur H, Kesharwani R, Verma G, et al. Cell death pathways in ischemic stroke and targeted pharmacotherapy. *Transl Stroke Res* (2020) 11:1185–202. doi: 10.1007/s12975-020-00806-z
47. Chen S, Zuo Y, Huang L, Sherchan P, Zhang J, Yu Z, et al. The MC4 receptor agonist RO27-3225 inhibits NLRP1-dependent neuronal pyroptosis via the ASK1/JNK/p38 MAPK pathway in a mouse model of intracerebral haemorrhage. *Br J Pharmacol* (2019) 176:1341–56. doi: 10.1111/bph.14639
48. Majidpoor J, Khezri Z, Rostamzadeh P, Mortezaee K, Rezaie MJ, Fathi F, et al. The expressions of NLRP1, NLRP3, and AIM2 inflammasome complexes in the contusive spinal cord injury rat model and their responses to hormonal therapy. *Cell Tissue Res* (2020) 381:397–410. doi: 10.1007/s00441-020-03250-5
49. Tan MS, Tan L, Jiang T, Zhu XC, Wang HF, Jia CD, et al. Amyloid-beta induces NLRP1-dependent neuronal pyroptosis in models of alzheimer's disease. *Cell Death Dis* (2014) 5:e1382. doi: 10.1038/cddis.2014.348
50. Gu R, Wang L, Zhou H, Wang X, Lenahan C, Qu H, et al. Rh-CXCL-12 attenuates neuronal pyroptosis after subarachnoid hemorrhage in rats via regulating the CXCR4/NLRP1 pathway. *Oxid Med Cell Longev* (2021) 2021:6966394. doi: 10.1155/2021/6966394
51. Mutua V, Gershwin LJ. A review of neutrophil extracellular traps (NETs) in disease: Potential anti-NETs therapeutics. *Clin Rev Allergy Immunol* (2021) 61:194–211. doi: 10.1007/s12016-020-08804-7
52. Sen T, Saha P, Gupta R, Foley LM, Jiang T, Abakumova OS, et al. Aberrant ER stress induced neuronal-IFNbeta elicits white matter injury due to microglial activation and T-cell infiltration after TBI. *J Neurosci* (2020) 40:424–46. doi: 10.1523/JNEUROSCI.0718-19.2019
53. Li P, Li M, Lindberg MR, Kennett MJ, Xiong N, Wang Y. PAD4 is essential for antibacterial innate immunity mediated by neutrophil extracellular traps. *J Exp Med* (2010) 207:1853–62. doi: 10.1084/jem.20100239